Journal of Ceramic Processing Research. Vol. 11, No. 5, pp. 547~551 (2010)

J O U R N A L O F
Ceramic Processing Research

The dependence of optical properties on the morphology and defects of nanocrystalline ZnO powders and their antibacterial activity

Sumetha Suwanboon[a,*], Pongsaton Amornpitoksuk[b], Phuwadol Bangrak[c], Apinya Sukolrat[d] and Nantakan Muensit[e]

[a]*Department of Materials Science and Technology, Faculty of Science, Prince of Songkla University, Hat Yai, Songkhla, 90112, Thailand*

[b]*Department of Chemistry and Center for Innovation in Chemistry, Faculty of Science, Prince of Songkla University, Hat Yai, Songkhla, 90112, Thailand*

[c]*School of Science, Walailak University, Nakhon Si Thammarat, Thailand, 80161, Thailand*

[d]*Scientific Equipment Center, Prince of Songkla University, Hat Yai, Songkhla, 90112, Thailand*

[e]*Department of Physics, Faculty of Science, Prince of Songkla University, Hat Yai, Songkhla, 90112, Thailand*

Nanocrystalline ZnO powders in a variety of shapes were synthesized through an easy precipitation method. Zinc salts, stabilizers and precipitating agents strongly affected the formation of the ZnO structure. The band gap value depended closely upon the amount of defects in various ZnO structures. The largest band gap value of 3.228 eV was obtained from ZnO nanorods with a crystallite size of 42 nm and a relative defect parameter of 0.099. The nanocrystalline ZnO particles can damage only *S. aureus*.

Key words: Precipitation, Defects, Optical properties, ZnO, Antibacteria.

Introduction

In recent years, much attention has been focused on the fabrication of ZnO nanostructures because of their unique physical and chemical properties. Naturally, ZnO is an n-type II-VI semiconductor with a wide band gap of 3.37 eV and a large exciton binding energy of 60 meV [1]. Therefore, ZnO can be used in many potential applications such in optoelectronic devices [2, 3], as rubber additives [4, 5], and for photocatalytic [6], antibacterial [7] and biomedical applications [8]. It has been well known that the properties of ZnO closely depend upon its size and shape. Thus, the strategy in morphological control has been concentrated in order to gain ZnO particles of various shapes such as spherical particles [9, 10], nanorods [1], nanowires [11], nanoflowers [12], and a porous ZnO structure [13] etc. To date, many techniques have been used to make ZnO nanostructures [14-18]. However, a precipitation method is nowadays a fashionable route because it is an easy method to control the precursor solution by a stabilizer as well as a high temperature and sophisticated equipments are not required. As far as we know, neither the formation of a flower-like ZnO structure via a TOA-assisted NH_4OH solution nor the formation of a porous ZnO structure through a CTAB-modified NaOH solution have been reported as yet. Therefore, we, herein, report a simple approach to prepare the ZnO nanostructures with different shapes from the CTAB and TOA-modified precipitating agent solutions and we also investigated the dependence of the band gap energy on the morphology and defects as well as the antibacterial activity towards *Staphylococcus aureus* and *Escherichia coli* was tested by an agar well diffusion assay.

*Corresponding author:
Tel : +66-74-28-8250
Fax: +66-74-28-8395
E-mail: ssuwanboon@yahoo.com

Experiment

Materials

The chemicals used in these experiments were analytical grade and they were used as received. Zinc acetate dihydrate ($Zn(CH_3COO)_2{\cdot}2H_2O$), zinc nitrate hexahydrate ($Zn(NO_3)_2{\cdot}6H_2O$), cetyltrimethyl ammonium bromide or CTAB ($C_{19}H_{42}BrN$) and trioctylamine or TOA ($C_{24}H_{51}N$) were purchased from Fluka. Ammonia solution (25% NH_4OH) and sodium hydroxide (NaOH) were supplied by Carlo Erba. Oxalic acid dihydrate ($C_2H_2O_4{\cdot}2H_2O$) was purchased from MERCK.

Preparation of ZnO nanorods (sample code: A)

6.4 g of NaOH (0.16 mol) was first dissolved in 100 ml of distilled water in a 600-ml conical flask. 7.2892 g of CTAB (0.02 mol) was then added into an aqueous NaOH solution and this solution was stirred continuously for 1 h until a homogeneous solution was obtained. 4.39 g of

$Zn(CH_3COO)_2{\cdot}2H_2O$ (0.02 mol) that was dissolved in 100 ml of distilled water, was finally dropped slowly into a CTAB-assisted NaOH solution. White precipitates were formed and they were heated at 70 °C for 1 h. The precipitates were filtered after being cooled and they were then rinsed with 300 ml of distilled water and 50 ml of absolute ethanol. After that they were dried at room temperature and calcined at 600 °C in air for 1 h.

Preparation of platelet-like ZnO nanoparticles (sample code: B)

1.6 g of NaOH (0.04 mol) was used in these experiments and the other processes were followed as in preparing the ZnO nanorods.

Preparation of ZnO nanoflowers (sample code: C)

6 ml of NH_4OH was first dissolved in 94 ml of distilled water in a 600-ml conical flask. 4.36 ml of TOA was then pipetted into a previous solution and this solution was further stirred at room temperature for 30 minutes. Finally, 4.39 g of $Zn(CH_3COO)_2{\cdot}2H_2O$ (0.02 mol) that was dissolved in 100 ml of distilled water, was added dropwise into a TOA-assisted NH_4OH solution. The other processes were followed as in preparing ZnO nanorods.

Preparation of a porous ZnO structure (sample code: D (without CTAB) and E (modified with CTAB)

20.1712 g of $C_2H_2O_4{\cdot}2H_2O$ (0.16 mol) was first dissolved in 100 ml of distilled water in each 600-ml conical flask for 1 h. 7.2892 g of CTAB (0.02 mol) was then added into an aqueous $C_2H_2O_4{\cdot}2H_2O$ solution while another $C_2H_2O_4{\cdot}2H_2O$ solution did not introduce the CTAB and these solutions were stirred continuously for 1 h until the homogeneous solutions were obtained. 5.9496 g of $Zn(NO_3)_2{\cdot}6H_2O$ (0.02 mol) that was dissolved in 100 ml of distilled water, was finally added dropwise into the $C_2H_2O_4{\cdot}2H_2O$ solution and the CTAB-assisted $C_2H_2O_4{\cdot}2H_2O$ solution. White precipitates were formed and they were stirred at room temperature for 1 h. The precipitates were filtered and they were then rinsed with 300 ml of distilled water and 50 ml of absolute ethanol. After that they were dried at room temperature and calcined at 600 °C in air for 1 h.

Sample characterizations

The structural and phase formation were identified by an X-ray diffractometer (XRD, X'Pert MPD, PHILIPS). The morphological study was evaluated by a scanning electron microscope (SEM, JSM-5800LV, JEOL) and the optical absorbance was determined by a UV-Vis spectrophotometer (UV-Vis 2450, Shimadzu).

Test of antibacterial activity

Antibacterial tests were performed by an agar well diffusion assay using a gram-positive bacterium *S. aureus* and gram-negative bacterium *E. coli* as indicator strains. The two species of bacteria grown individually on nutrient agar plates at 37 °C for 16-18 h were resuspended in 0.85% sterile saline equivalent to a turbidity of standard McFarland No. 0.5 with approximate 1.5×10^8 colony forming units/ml (CFU/ml). The suspension of testing bacteria was spread on the Mueller-Hinton agar plate and left at room temperature for 5 minutes so as to allow the moisture from the inocula to absorb into the medium. Wells were punched in the agar with a sterile cock-borer of 9 mm diameter. The ZnO suspensions (2.5 mg/ml) were filled directly into the wells of the agar plates inoculated with indicator bacteria. The agar plates were left at room temperature for 15 minutes and then incubated at 37 °C for 16 h and the diameters of the inhibition zones were finally measured in millimetre.

Results and Discussion

Structural study

The calcined ZnO samples were identified by the XRD technique and the results are shown in Fig. 1

The XRD patterns of all samples were in good agreement with the pattern of the ZnO standard with a space group of $P6_3mc$ and lattice parameters: $a = 0.3250$ and $c = 0.5207$ nm according to the JCPDS number of 36-1451. Therefore, it could be concluded that the calcined samples are a pure ZnO phase. Based on the XRD results, the average crystallite size of ZnO was determined by Scherrer's formula [19] ($D = k\lambda/\beta\cos\theta$, where D is the average crystallite size, k is a constant equal to 1, λ is the wavelength of the X-rays used, β is a line width in radians at half maximum intensity and θ is the Bragg angle). The calculated crystallite sizes are given in Table 1.

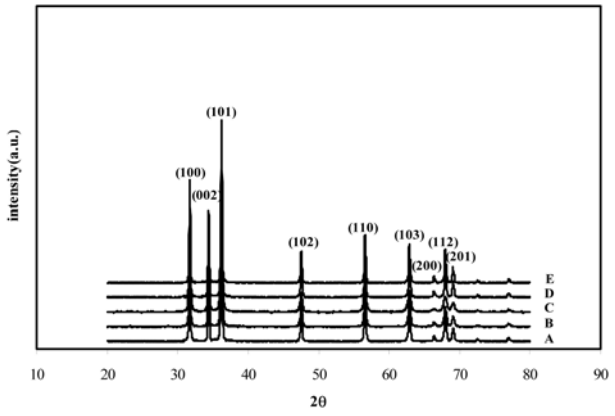

Fig. 1. XRD patterns of ZnO samples with different shapes A: nanorod, B: platelet, C: nanoflower, D and E: porous structure.

Table. 1. The data of structural and optical properties of ZnO samples

sample code	crystallite size (nm)	lattice parameter (nm)		E_g (eV)	particle shape	1/slope
		a	*c*			
A	42	0.3253	0.5211	3.228	rod	0.099
B	41	0.3254	0.5213	3.171	platelet	0.129
C	34	0.3254	0.5212	3.174	flower	0.111
D	46	0.3254	0.5212	3.198	porous	0.127
E	54	0.3254	0.5213	3.204	porous	0.072

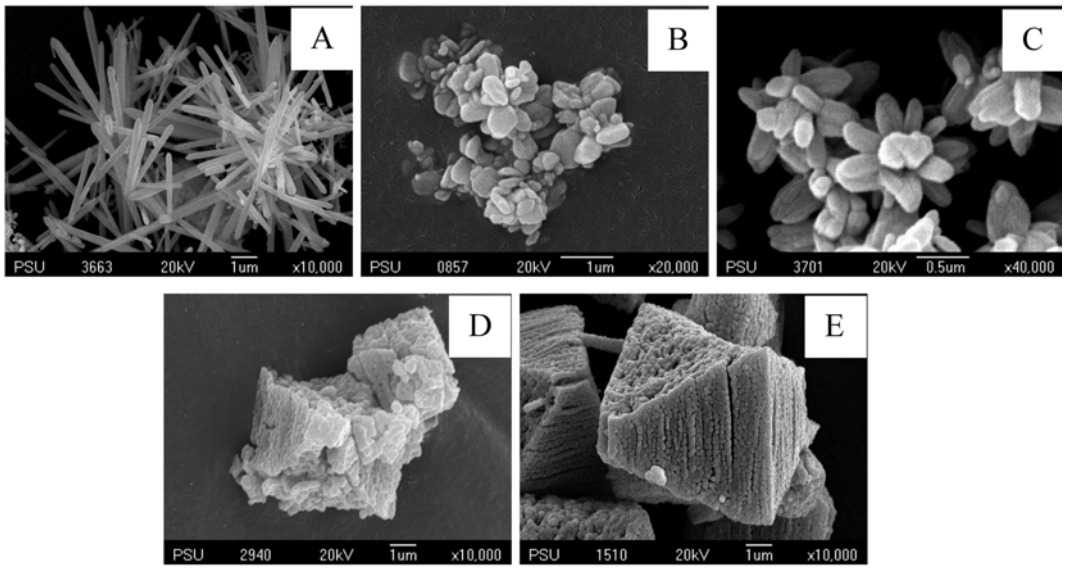

Fig. 2. SEM images of calcined ZnO samples with different shapes.

It was evident that the crystallite size of calcined ZnO samples strongly depended upon the conditions used. The smallest crystallite size of about 34 nm was observed when TOA and ammonia solution were used as a capping agent and a precipitating agent, respectively. Not only the crystallite size, but also the particle shape was influenced from the conditions selected as seen in the SEM images in Fig. 2.

It was clearly seen that different shapes of ZnO nanostructures were formed when different preparation conditions were used in this study. Rod structures (sample A) were shaped when 0.16 mol NaOH solution was used while the platelet-like shape (sample B) was formed when the amount of NaOH was reduced to 0.04 mol. Here, the dependence of ZnO shape on the concentration of the aqueous NaOH solution could be explained by different growth rate of crystal planes. Under a strong alkaline solution (sample A), $Zn(OH)_2$ was formed and was completely dissolved to $Zn(OH)_4^{2-}$. The $Zn(OH)_4^{2-}$ could act as a growth unit with different growth rates of the planes as follows [20]:

$$v_{(0001)} > v_{(\bar{1}0\bar{1}\bar{1})} > v_{(\bar{1}010)} > v_{(\bar{1}011)} > v_{(000\bar{1})}.$$

If the degree of supersaturation exceeds the critical value, the ZnO nuclei started to nucleate in the solutions and this was followed with a subsequent growth in the form of a rod structure under the driving force of the surface energy, electrostatic force [21] etc. Furthermore, the $N(CH_3)_3^+$ or CTA^+ groups could encapsulate on the side faces of ZnO, giving rise to a rapid growth along the *c*-axis and thus a smaller rod was shaped. On the other hand, a platelet-like shape was formed with a lower NaOH concentration (0.04 mol). It is proposed that the $Zn(OH)_2$ could not dissolve completely and the $Zn(OH)_2$ played an important role in controlling the growth of the platelet-like ZnO structure. In this case, the growth along the *c*-axis was prevented and the growth could occur along the slowest growth rate of the $(000\bar{1})$ plane and the side faces. To date, it has been well known that an explanation of the growth process and mechanism for ZnO formation has not been clear enough. However, under a mild alkaline solution with a presence of CTAB, a growth process of ZnO via the following reactions could be accepted [21, 22]:

$$Zn^{2+} + 2OH^- + CTA^+ \leftrightarrow Zn(OH)_2\text{–}CTA^+ \quad (1)$$

$$Zn(OH)_2\text{–}CTA^+ \leftrightarrow ZnO\text{–}CTA^+ + H_2O \quad (2)$$

$$ZnO\text{–}CTA^+ \overset{\Delta}{\leftrightarrow} ZnO \quad (3)$$

Owing to the smaller solubility of ZnO compared to $Zn(OH)_2$, the $Zn(OH)_2$ consequently tended to be transformed into ZnO. In contrast, ZnO was formed under a strong alkaline solution via the following reactions [23]:

$$Zn^{2+} + 2OH^- + CTA^+ \leftrightarrow Zn(OH)_2\text{–}CTA^+ \quad (4)$$

$$Zn(OH)_2\text{–}CTA^+ + 2OH^- \leftrightarrow Zn(OH)_4^{2-}\text{-}CTA^+ \quad (5)$$

$$Zn(OH)_4^{2-}\text{–}CTA^+ \rightarrow ZnO\text{-}CTA^+ + H_2O + 2OH^- \quad (6)$$

$$ZnO\text{-}CTA^+ \overset{\Delta}{\rightarrow} ZnO \quad (7)$$

Considering the mechanism for formation of the flower-shaped ZnO structure (sample C), it has been found that an organic amine and an ammonium solution were a key parameter influencing the formation of a flower-like structure [24, 25]. Here, TOA could primarily adsorb on the (0001) plane of ZnO nuclei and the growth along (0001) plane or the *c*-axis was greatly retarded which was similar to the effect of TEA [26, 27]. Moreover, the adsorption of TOA on the (0001) plane was not uniform and the adsorption always deviated from the center of the plane. So, its shape was similar to the petals. In this study, the ZnO formation can be depicted by the following reactions:

$$NH_3 + H_2O \leftrightarrow NH_3.H_2O \leftrightarrow NH_4^+ + OH^- \quad (8)$$

$$Zn^{2+} + 2OH^- + TOA \leftrightarrow Zn(OH)_2{-}TOA \quad (9)$$

$$Zn(OH)_2{-}TOA + 2OH^- \leftrightarrow Zn(OH)_4^{2-}TOA \quad (10)$$

$$Zn(OH)_4^{2-}{-}TOA \rightarrow ZnO\text{-}TOA + H_2O + 2OH^- \quad (11)$$

$$ZnO\text{-}TOA \xrightarrow{\Delta} ZnO \quad (12)$$

For construction of a porous ZnO structure, it was clearly observed that CTAB did not affect the shape of ZnO under a strong acidic solution as clearly seen from SEM images for samples D and E in Fig. 2. The SEM images showed that a porous ZnO structure was constructed with well-aligned spherical particles with a size of about 200 nm. In this study, a porous ZnO structure was formed via the ZnC_2O_4 intermediate that can be described by the following reactions [28]:

$$Zn^{2+} + C_2O_4^{2-} \rightarrow ZnC_2O_4.2H_2O \quad (13)$$

$$ZnC_2O_4.2H_2O + 1/2O_2 \xrightarrow{\Delta} ZnO + 2CO_2 + 2H_2O \quad s(14)$$

Optical study

As far as ZnO nanomaterial is concerned, the investigation of its optical properties has been of interest because ZnO has a great potential in many applications. In this study, the absorbance of all calcined samples was measured and the results are presented in Fig. 3(a).

The ZnO samples prepared in these experiments showed a highly transparent mode in the visible region and the absorption edge of all samples was lower than 400 nm depending upon their shape and size. To estimate the band gap value (E_g), the curve of $(\alpha h\upsilon)^2$ versus $h\upsilon$ or Kubelka-Munk model [29] was plotted as displayed in Fig. 3(b). The extrapolation of the straight line down to zero on the *x*-axis (where E or $h\upsilon = E_g$) is an E_g value for each sample and the results acquired are given in Table 1. Interestingly, the E_g values are strongly dependent upon the ZnO shape. When alkaline solutions were utilized to germinate the ZnO nuclei, the largest E_g value of 3.228 eV was obtained from the rod structure (sample A) even though it has the largest crystallite size. This might be due to a lower defect concentration in the crystals of ZnO for sample A. To evaluate the amount of defects in ZnO crystals, a curve of $\ln(\alpha)$ versus $h\upsilon$ was plotted and given in Fig. 4 and a reciprocal values that referred to the amount of defects were shown in Table 1.

It is clearly seen that the reciprocal values of the slopes from the linear part are 0.099, 0.129 and 0.111 for samples A, B and C, respectively. Thus, it could be concluded that the ZnO particles with different shapes have a different content of defects and these defects had strongly affected the E_g value. From the results obtained, the E_g value of all samples was smaller than that of the E_g value of a ZnO single cystal (3.37 eV), this might be because the E_g values in these experiments were due to the electronic transition from the filled valence states to energy levels of defects instead of the electronic transition from the filled valence band to the empty conduction band as usual. For this reason, it is reasonable to summarize that a shape with larger crystallite size, but a smaller amount of defects gave a

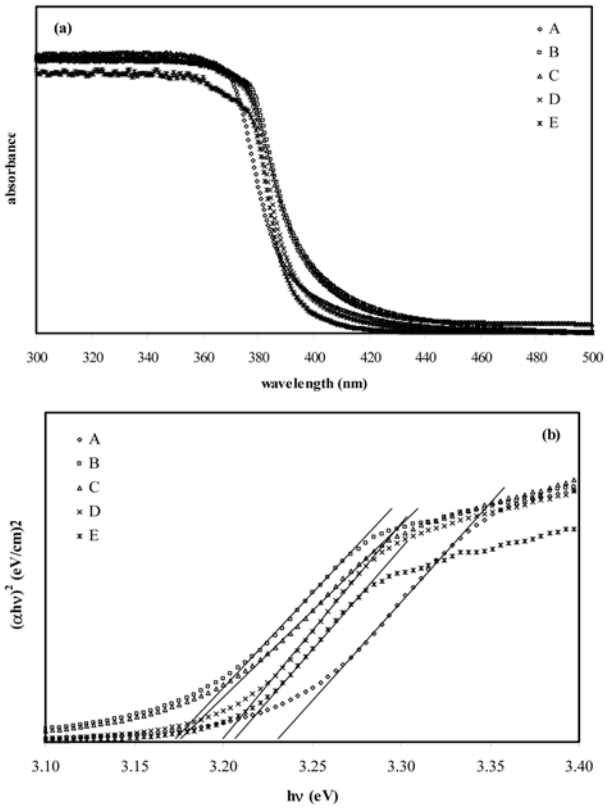

Fig. 3. (a) absorbance spectra, and (b) evolution of the $(\alpha h\upsilon)^2$ vs. $h\upsilon$ curves of the calcined ZnO samples.

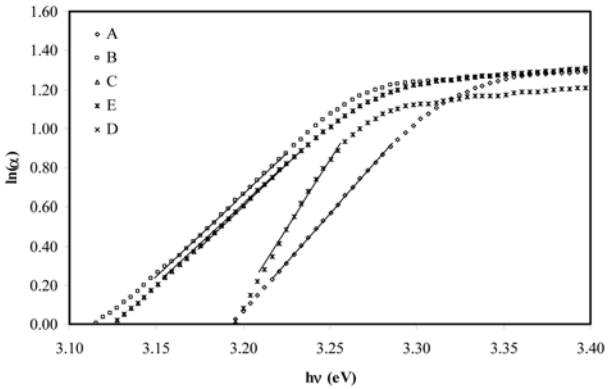

Fig. 4. The plot of $\ln(\alpha)$ vs. $h\upsilon$ of calcined samples.

significantly larger E_g value when the ZnO particles were synthesized by alkaline solutions. Similarly, as the ZnO particles were fabricated under strong acidic conditions (samples D and E), a porous ZnO structure (sample E) with a larger crystallite size, but a smaller amount of defects also showed a larger E_g value.

Antibacterial activity

In this study, the antibacterial activity of ZnO suspension towards *S. aureus* and *E. coli* was tested by an agar well diffusion method and the results are given in Table 2.

From the results obtained, all the ZnO samples synthesized in these experiments can damage only *S. aureus*. It is well known that the gram-positive bacteria (*S. aureus*) and gram-

Table 2. The effect of nanocrystalline ZnO powders on inhibition of *S. aureus* and *E. coli* by an agar well diffusion method

sample code	Inhibition zone diameter (mm)	
	S. aureus	*E. coli*
A	13	none
B	13	none
C	12	none
D	14	none
E	14	none

negative bacteria (*E. coli*) have different basic structures. The outside rigid cell wall of gram-negative bacteria is composed of lipopolysaccharides instead of phospholipids. The lipopolysccharides normally form an extra physical barrier to penetration by the ZnO particles [30]. For this reason, the ZnO can damage better *S. aureus*. The bacterial tests were done under dark conditions, and a possible mechanism for the damage of the bacteria could be due to the penetration of ZnO particles into the membrane cell wall to damage the bacteria from the interior [31]. From this study, the ZnO can penetrate into the cell wall of *S. aureus*, but they can not penetrate into the cell wall of *E. coli* according to the different compositions of membrane cell walls as previously mentioned. Therefore, ZnO particles can damage only *S. aureus*.

Conclusions

Rod-like and platelet-like ZnO structures were shaped from the $Zn(CH_3COO)_2.2H_2O$ and the CTAB-modified NaOH solutions under strong and mild alkaline solutions, respectively. A flower-like ZnO shape was constructed from the $Zn(CH_3COO)_2{\cdot}2H_2O$ and the TOA-modified NH_4OH solutions. A porous ZnO structure was synthesized from $Zn(NO_3)_2{\cdot}6H_2O$ and $C_2H_2O_4{\cdot}2H_2O$ solutions under strong acidic conditions. The value of the optical band gap strongly depended upon the amount of defects and the shape of ZnO particles. The ZnO particles prepared under all conditions in this study could damage only *S. aureus*.

Acknowledgements

The authors would like to acknowledge the financial support from the Thailand Research Fund (TRF) under the contract number MRG5280125 and the Research, Development and Engineering (RD&E) fund through The National Nanotechnology Center (NANOTEC), The National Science and Technology Development Agency (NSTDA), Thailand (Project No. NN-B-22-FN8-19-52-21) to Prince of Songkla University. The authors also would like to acknowledge the Center for Innovation in Chemistry (PERCH-CIC), Commission on Higher Education, Ministry of Education.

References

1. J. Zhao, Z.G. Jin, X.X. Liu and Z.F. Liu, J. Eur. Ceram. Soc. 26[16] (2008) 3745-3752.
2. M. Purica, E. Budianu and E. Rusu, Microelectron. Eng. 51-52 (2002) 425-431.
3. C.Y. Hsu and C.H. Tsang, Sol. Energy Mater. Sol. Cells 92[5] (2008) 530-536.
4. X. Xiao, C. Li, D. Yang, and S. He, Nucl. Instrum. Methods Phys. Res., Sect. B. 266[15] (2008) 3375-3380.
5. M. Sugano, M. Tsubosaka, S. Shimizu, M. Fujita, T. Fukumoto, K. Hirano and K. Mashimo, Energy Fuels. 22[3] (2008) 1986-1990.
6. A. Dodd, A. Mckinley, T. Tsuzuki, and M. Saunders, J. Eur. Ceram. Soc. 29[1] (2009) 139-144.
7. L. Zhang, Y. Ding, M. Povey and D. York, Prog. Nat. Sci. 18[8] (2008) 939-944.
8. D. Guo, C. Wu, H. Jian, Q. Li, X. Wang and B. Chen, J. Photochem. Photobiol., B. 93[3] (2008) 119-126.
9. N. Uekawa, S. Tahii, T. Kojima and K. Kakegawa, Mater. Lett. 61[8-9] (2007) 1729-1734.
10. J.K. Yong, H.K. Hun, L.M. Chang and B.S. Kwang, J. Ceram. Process. Res. 3[3] (2002) 146-149.
11. T.J. Hsueh, C.L. Hsu, S.J. Chang and I.C. Chen, Sens. Actuator B. 126[2] (2007) 473-477.
12. J.M. Jang, C.R. Kim, H. Ryu, M. Razeghi and W.G. Jung, J. Alloys Compd. 463[1-2] (2008) 503-510.
13. J. Zheng, Z.Y. Jiang, Q. Kuang, Z.X. Xie, R.B. Huang and L.S. Zheng, J. Solid State Chem. 182[1] (2009) 115-121.
14. J.E. Rodriguez-Paez, A.C. Caballero, M. Villegas, C. Moure, P. Duran and J.F. Fermandez, J. Eur. Ceram. Soc. 21[7] (2001) 925-930.
15. X.M. Sun, X. Chen, Z.X. Deng and Y.D. Li, Mater. Chem. Phys. 78[1] (2002) 99-104.
16. W.S. Kim, H.W. Kim and N.H. Kim, Physica B. 334[3-4] (2003) 343-346.
17. P.T. Hsieh, Y.C. Chen, K.S. Kao, M.S. Lee and C.C. Cheng, J. Eur. Ceram. Soc. 27[13-15] (2007) 3815-3818.
18. T. Masaki, S.J. Kim, H. Watanabe, K. Miyamoto, M. Ohno and K.H. Kim, J. Ceram. Process. Res. 4[3] (2003) 135-139.
19. T. Ratana, P. Amornpitoksuk, T. Ratana and S. Suwanboon, J. Alloys Compd. 470[1-2] (2009) 408-412.
20. W.J. Li, E.W. Shi, W.Z. Zhong and Z.W. Yin, J. Cryst. Growth. 203[1-2] (1999) 186-196.
21. J. Xie, P. Li, Y. Li, Y. Wang and Y. Wei, Mater. Chem. Phys. 114[2-3] 943-947.
22. Q. Ahsanulhaq, S.H. Kim, J.H. Kim and Y.B. Hahn, Mater. Res. Bull. 43[12] (2008) 3483-3489.
23. R. Yi, N. Zhang, H. Zhou, R. Shi, G. Qiu and X. Liu, Mater. Sci. Eng., B. 153[1-3] (2008) 25-30.
24. M. Epifani, Mater. Lett. 61[14-15] (2007) 3100-3102.
25. Y. Masuda, N. Kinoshita and K. Koumoto, Electrochim. Acta 53[1] (2007) 171-174.
26. P. Li, Y. Wei, H. Liu and X.K. Wang, J. Solid State Chem. 178[3] (2005) 855-860.
27. P. Li, H. Liu, Y.F. Zhang, Y. Wei and X.K. Wang, Mater. Chem. Phys. 106[1] (2007) 63-69.
28. K.G. Kanade, B.B. Kale, R.C. Aiyer and B.K. Das, Mater. Res. Bull. 41[3] (2006) 590-600.
29. T. Rattana, S. Suwanboon, P. Amornpitoksuk, A. Haidoux and P. Limsuwan, J. Alloys Compd. 480[2] (2009) 603-607.
30. P. Lowrie and S. Wells, in "Microbiology and Biotechnology" (Cambridge, 2000) p. 2.
31. L. Zhang, Y. Jiang, Y. Ding, M. Povey and D. York, J. Nanopart. Res. 9 (2007) 479-489.